Chapter 8
Pre-Main Sequence Evolution

As can be seen from the calculations of cloud collapse described in Sect. 7.2, stars with mass $M > 3M_\odot$ appear in the optical range immediately near to the main sequence. Objects of lower mass exist for part of the time as optical stars with radiation due to gravitational contraction energy. Consider evolution of a star from its appearance in the optical region until it reaches the main sequence, and its central temperature becomes sufficiently high to initiate a nuclear reaction converting hydrogen into helium (see review [105]).

8.1 Hayashi Phase

The pre-main sequence evolution of stars takes place at not very high temperatures, when a non-full ionization of matter and large opacity cause such stars to be almost convective. This fact was first established by Hayashi [461, 462], who took into account a convection in constructing evolutionary tracks for contracting stars in the HR diagram (see Fig. 7.6 from [930] plotted with the aid of calculations from [485]). Evolutionary calculations in the papers listed below have been made by the Henyey method. This method is based on the division of the stellar mass into J intervals, and writing the differential equations describing static equilibrium, mass conservation, and heat transfer in a difference form. The solution of linearized difference equations is obtained by the "back substitution method", which is very convenient for numerical computations (see Sect. 6.1, Vol. 1).

8.1.1 Nuclear Reactions

Though reaction rates are insufficient for establishing a thermal equilibrium of the star, some contribution into the heat balance of the star in the phase of gravitational contraction to the main sequence can nevertheless be done by reactions with light elements. Calculations in [462] include the burning of ^2D, ^7Li, ^9Be, small amounts of which were formed at the beginning of the Universe expansion. The rate of energy

release in the $^2D(p, \gamma)^3He$ reaction is given in Sect. 4.2, Vol. 1. For the two other reactions, we have from [258, 393]

$$^7Li(p, \alpha)^4He, \qquad Q_6 = 17.346,$$

$$N_A\langle^7Li\,p\rangle_\alpha = 1.096 \times 10^9 \; T_9^{-2/3} \exp\left(-\frac{8.472}{T_9^{1/3}}\right)$$

$$- 4.830 \times 10^8 \; T_{9A}^{5/6} \; T_9^{-3/2} \exp\left(-\frac{8.472}{T_{9A}^{1/3}}\right)$$

$$+ 1.06 \times 10^{10} \; T_9^{-3/2} \exp\left(-\frac{30.442}{T_9}\right),$$

$$T_{9A} = T_9/(1 + 0.759 \, T_9), \tag{8.1}$$

$$\epsilon_{^7Li\,p\alpha} = 2.391 \times 10^{18} x_{^7Li} \, x_H \, \rho N_A\langle^7Li\,p\rangle_\alpha;$$

and

$$^9Be(p, \alpha)^6Li, \qquad Q_6 = 2.126,$$

$$N_A\langle^9Be\,p\rangle_\alpha = 2.11 \times 10^{11} \; T_9^{-2/3} \exp\left[-\frac{10.359}{T_9^{1/3}} - \left(\frac{T_9}{0.520}\right)^2\right]$$

$$\times \left(1 + 0.040 \, T_9^{1/3} + 1.09 \, T_9^{2/3} + 0.307 \, T_9\right.$$

$$\left. + 3.21 \, T_9^{4/3} + 2.30 \, T_9^{5/3}\right)$$

$$+ \frac{4.51 \times 10^8}{T_9} \exp\left(-\frac{3.046}{T_9}\right) + \frac{6.70 \times 10^8}{T_9^{3/4}} \exp\left(-\frac{5.160}{T_9}\right),$$

$$\tag{8.2}$$

$$\epsilon_{^9Be\,p\alpha} = 2.279 \times 10^{17} x_{^9Be} \, x_H \, \rho N_A\langle^9Be\,p\rangle_\alpha.$$

Detailed calculations for the pre-main sequence evolution of stars with masses of 0.5, 1.0, 1.25, 1.5, 2.25, 3.0 $M_\odot$ have been performed in [485]. They include reactions of the pp-cycle and the ^{12}C, ^{14}N, and ^{16}O burning in the CNO cycle. The corresponding reactions and the energy release per reaction Q_6 (in MeV) are

$$p\,(p, e^{+\,\circ})^2D, \quad \text{with } Q_6 = 1.192;$$

$$^3He\,(^3He, 2p)^4He, \quad \text{with } Q_6 = 12.860;$$

$$^{12}C\,(p, \gamma)^{13}N, \quad \text{with } Q_6 = 1.944;$$

$$^{14}N\,(p, \gamma)^{15}O, \quad \text{with } Q_6 = 7.297;$$

$$\text{and } ^{16}O\,(p, \gamma)^{17}F, \quad \text{with } Q_6 = 0.600.$$

The reaction rates and energy release rates of the above reactions are given in Sect. 4.2, Vol.1. The notations used in (8.1)–(8.3) are: $T_9 = T/10^9$ K, $\langle 01 \rangle \equiv \langle \sigma v \rangle_{01}$ (cm^3 s^{-1}) is the reaction rate, σ is a cross-section of the reaction, v is a relative velocity, $\langle \rangle$ denotes averaging of the corresponding values of reacting nuclei over the energy distributions (Maxwellian), $N_A = 6.02252 \times 10^{23}$ g^{-1} is the Avogadro number. These notations are common in the literature, following [392], see also Sect. 4.1, Vol. 1.

From [258, 459] one has the reaction rate

$$^4\text{He}(^3\text{He}, \gamma)^7\text{Be}, \qquad Q_6 = 1.588,$$

$$N_A \langle ^4\text{He}\,^3\text{He} \rangle_\gamma = 5.61 \times 10^6\, T_9^{-3/2}\, T_{9A}^{5/6} \exp\left(-\frac{12.826}{T_{9A}^{1/3}}\right), \qquad (8.3)$$

$$T_{9A} = T_9/(1 + 0.0495\, T_9),$$

$$\epsilon_{^4\text{He}\,^3\text{He}_\gamma} = 1.277 \times 10^{17} x_{^4\text{He}}\, x_{^3\text{He}}\, \rho N_A \langle ^4\text{He}\,^3\text{He} \rangle_\gamma.$$

For other reactions of pp- and CNO-cycles, the heat release is taken into account in [485], but they are assumed to proceed instantaneously. For example, the reaction $\text{p}\,(\text{p}, \text{e}^+ v)^2\text{D}$ is assumed to produce ^3He yielded by the fast $^2\text{D}(\text{p},\gamma)^3$ He reaction with $Q_6 = 5.494$, rather than ^2D, while the $^{12}\text{C}(\text{p},\gamma)^{13}\text{N}$ reaction eventually produces ^{14}N, because the reactions $^{13}\text{N} \rightarrow ^{13}\text{C} + \text{e}^+ + v$ with $Q_6 = 1.51$, and $^{13}\text{C}(\text{p},\gamma)^{14}\text{N}$ with $Q_6 = 7.551$ proceed more rapidly, (see Sect. 4.2, Vol. 1). The $^6\text{Li}\,(\text{p}, \alpha)^3\text{He}$, $^{10}\text{B}\,(\text{p}, \alpha)^7\text{Be}$ and $^{11}\text{B}\,(\text{p}, \alpha)^8\text{Be}$, reactions, which are of little importance in the energy release, are also considered in [444]. All the reaction rates used in the calculations have been multiplied by a screening factor increasing the reaction rates due to a reduction in the electric repulsion between nuclei (see Sect. 4.5, Vol. 1). The times of approach to the main sequence t_{ms} for stars of diverse masses are [485]:

t_{ms}, yr	2.514(6)	5.855(6)	1.821(7)	2.954(7)	5.016(7)	1.550(8)
$M/M_\odot$	3.0	2.25	1.5	1.25	1.0	0.5

We now clarify the reasons for the appearance of extrema on evolutionary tracks [485] (Fig. 7.6). The first minimum to the right is caused by the growth of the radiative core. Further contraction of stars with $M \geq 0.8\, M_\odot$ is accompanied by a rapid accumulation of ^3He produced in the H and ^2D burning in the reactions $\text{p}(\text{p},\text{e}^+ v)^2\text{D}$, $^2\text{D}(\text{p},\gamma)^3\text{He}$, and by a diminution of ^{12}C in the reaction $^{12}\text{C}(\text{p},\gamma)^{13}\text{N}$ (see Sect. 4.2, Vol. 1) that enhance the pressure gradient slowing the star contraction and lead to convection development in the centre. As a result, the star passes over the peak of its luminosity; a star with $M \leq M_\odot$ reaches the main sequence after the disappearance of the convective core.

For $M = 1.5\, M_\odot$, a decrease in the concentration of ^{12}C reduces the fractional contribution of the nuclear energy into the luminosity. The gravitational energy begins to play a more important role when the star has not reached the main

sequence, which causes the luminosity to reach a second minimum and to increase subsequently. After the concentration of ^{12}C has reached an equilibrium value, the role of the nuclear energy becomes more important for the second time, the contraction slows down, the luminosity reaches a maximum once again, and the star reaches the main sequence with a non-zero mass of its convective core. The appearance of new extrema near the main sequence for $M \geq 1.25\,M_\odot$ is due to an increased role of the CNO-cycle of hydrogen burning in stars of large mass compared to the pp-cycle.

Calculations of pre-main sequence evolution for masses $M = (0.5–2.5)\,M_\odot$ for two different metallicities ($Z = 0.02$ and 0.04) and different convection factors α_p from (8.6) have shown [390] a high sensitivity of results to the input parameters. It was concluded that it is quite difficult to determine masses of T Tauri stars with a precision of better than $0.3M_\odot$. The same conclusion holds, to a lesser extent, for age determination, especially if the metallicity of the observed star is not accurately measured.

8.1.2 Non-Ideality of Matter

In studies of the evolution of low-mass stars, $M \leq 0.2M_\odot$, Coulomb corrections to the equation of state and ionization by pressure have been taken into account ([479], see Sect. 1.4, Vol. 1). Simplified techniques have been used in [380, 443–446] in order to include the ionization by pressure. The level shift had been taken into account by using a factor $\phi(r_0) = \exp(r_p/r_0)^3$ in the Saha equation [617], which is written in this case as

$$\frac{y_{i,j-1}}{y_{ij}} = n_e \frac{g_{i,j-1}}{2g_{ij}} \left(\frac{2\pi\hbar^2}{m_e kT} \right)^{3/2} e^{I_{ij}/kT} e^{(r_p/r_0)^3} \equiv n_e K(T). \tag{8.4}$$

Here $I_{ij} = \epsilon_{i,j-1} - \epsilon_{ij}$ is the ionizaton energy (potential) of the j-th electron, and $I_{i0} = 0$; y_{ij} is a fraction of a j-folded ionization of the i-th element; g_{ij} is a statistical weight of the i-th element in the ionization state j. Moreover,

$$r_0 = \left(\frac{3}{4\pi n_i} \right)^{1/3}$$

is the mean interion separation, and

$$r_p = \gamma \frac{\hbar^2}{m_e e^2}$$

is the quantity close to the Bohr radius and given in Table 8.1 from [443].

The degeneracy of electrons has been included in $K(T)$ in the right-hand side of (8.4) by using, as in [479], the relevant expression for the chemical potential μ_{te} of

Table 8.1 Radii r_p

Element	$r_{p,\,A}$	Element	$r_{p,\,A}$	Element	$r_{p,\,A}$
H	0.795	N	0.53	Ni	1.07
H^-	2.12	O	0.45	Ca	2.03
H_2	1.18	C	0.66	Al	1.21
H_2^+	1.30	S	0.82	Na	1.55
He	0.475	Si	1.06	K	2.06
He^+	0.400	Fe	1.22		
Ne	0.32	Mg	1.32		

electrons in the basic relation determining the ionization equilibrium

$$\mu_{t,i,j-1} = \mu_{t,ij} + \mu_{te}, \tag{8.5}$$

where $\mu_{t,ij}$ is the chemical potential of the i-th element in the ionization state j (see also Sect. 1.2, Vol. 1).

### 8.1.3 Evolution of Low-Mass Stars, Minimum Mass of a Star on the Main Sequence, Role of Various Factors

Evolutionary calculations of low-mass stars in approach to the main sequence have been made by the Henyey method. Not only diverse methods of allowing for the non-ideality have been used in these calculations but a variety of chemical compositions and coefficients α determining the mixing length l have also been considered. Here, $\alpha \equiv \alpha_p$ is connecting the pressure scale height H_p with l, so that

$$l = \alpha_p H_p = \alpha_p \frac{P}{|dP/dr|} \tag{8.6}$$

(see Sect. 3.1, Vol. 1). Evolutionary tracks as functions of α have been studied in [444]. The effect of specified boundary conditions, deuterium burning and an applied method of allowing for the non-ideality on the evolutionary track of a star contracting to the main sequence have been investigated in [445, 446].

The evolutionary tracks of stars calculated in [380] from the Hayashi boundary are shown in Fig. 8.1. The chemical composition corresponds to $x_H = 0.7$, $x_{He} = 0.27$, $x_Z = 0.03$. The atmosphere and envelope are calculated similarly to [769] by solving equations for the static atmosphere with an approximate description of optically thin layers with $\tau < 1$. This description gives a smooth transition to the equation for the radiative heat conductivity, valid for deep layers inside the photosphere (see Sects. 2.2.3 and 6.1, Vol. 1). The envelope mass equals 3% of the stellar mass. The convection is included according to the mixing length theory with $l = P/\nabla P$ ($\alpha = 1$), the non-ideality similarly to [443], see (8.4); the hydrogen burning reactions in the proton cycle with the inclusion of screening are also considered in this paper.

Fig. 8.1 Tracks for
spherically symmetric stars
with masses of 0.07, 0.09 and
0.11 $M_\odot$ in the HR diagram
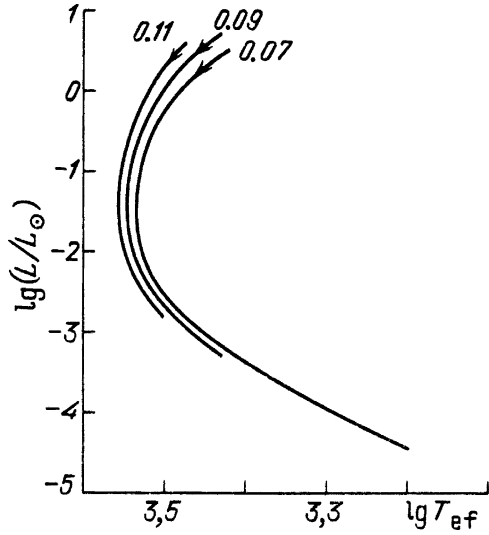
Table 8.2 Parameters of stars with maximum central temperatures T_c

$\frac{M}{M_\odot}$	t, yr	lg T_c	lg ρ_c	$(\beta - \alpha)_c$	$\frac{L_{grav}}{L}$	lg T_{ef}	lg $\frac{L}{L_\odot}$	lg $\frac{R}{R_\odot}$
0.07	2.2(8)	6.448	2.5	4.2	0.96	3.41	−3.27	−0.94
0.08	3.3(8)	6.524	2.62	4.2	0.78	3.42	−3.28	−0.96

Table 8.3 Parameters of stars on the main sequence

$\frac{M}{M_\odot}$	t, yr	lg T_c	lg ρ_c	$(\beta - \alpha)_c$	lg T_{ef}	lg $\frac{L}{L_\odot}$	lg $\frac{R}{R_\odot}$
0.09	1.6(9)	6.596	2.74	4.41	3.42	−3.30	−0.27
0.10	8.9(8)	6.645	2.67	3.35	3.46	−3.07	−0.93
0.11	5.7(8)	6.684	2.59	2.57	3.49	−2.88	−0.89

According to the calculations, stars with masses of $0.09 M_\odot$, $0.1 M_\odot$ and $0.11 M_\odot$ reach the main sequence, whereas stars with mass $0.08 M_\odot$ and less reach a state with a maximum central temperature T_c during contraction and subsequently cool, transforming into degenerate hydrogen dwarfs.

Table 8.2, from [380], gives parameters of stars with maximum T_c, while Table 8.3 presents parameters of stars on the main sequence, when $L_{grav}/L = 0.01$.

The central values of

$$\alpha = \frac{M_e C^2}{kT} \qquad \beta = \frac{M_{te}}{kT} \tag{8.7}$$

are used to determine a level of electron degeneracy. Large positive values of $(\beta - \alpha)$ correspond to highly degenerate, and large negative ones determine non-degenerate electrons (see Sect. 1.2, Vol. 1).

Fig. 8.2 $\lg T_c$ as a function of $\lg \rho_c$ for a star with initial mass 0.07 $M_\odot$ and the mass increase rate $10^{-12} M_\odot/\mathrm{yr}$ near the main sequence. The *dashed curves* represent spherically symmetric stars with constant masses of 0.07, 0.08, 0.09, 0.10 and 0.11 $M_\odot$
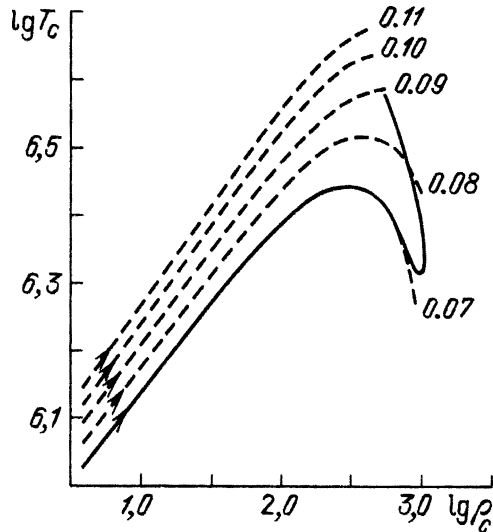
The minimum mass of a star on the main sequence is in the interval $0.08 M_\odot \leq M \leq 0.09 M_\odot$. The low-mass stars reaching the main sequence (Table 8.2) conserve the full convectivity state. The line in the HR diagram along which a fully convective star of a given mass evolves in the absence of degeneracy is obtained in [461, 462] and is called the Hayashi boundary or Hayashi track. It is shown in [461,462] that the presence of a radiative core shifts the star to the left of this boundary (see Fig. 7.6). In the presence of accretion, a low-mass star with $M < M_{\min}$ may turn back to the main sequence upon going over the T_c minimum. A typical evolutionary track is shown in Fig. 8.2 for the initial mass $0.07 M_\odot$ and accretion rate $10^{-12} M_\odot/\mathrm{yr}$.

Models for low-mass stars with a small-scale magnetic field included by adding the magnetic pressure term

$$P_m = C\rho^{4/3} \tag{8.8}$$

to the equation of state have been calculated in [379]. The magnetic pressure reduces the temperature needed for equilibrium of a star of the same mass and its density and increases the minimum mass of the star reaching the main sequence: $M_{\min}^{(\mathrm{H})} > M_{\min}$. Calculations with $C = 2.4 \times 10^{13}$ in (8.8) have yielded the value $M_{\min}^{(\mathrm{H})} = 0.12 M_\odot$ (see Table 8.4). Note that a star with $M = 0.12 M_\odot$ reaches the main sequence upon going over the central temperature maximum. The rotation effect on $M_{\min}$ is considered in Sect. 8.2.

8.1.4 Evolutionary Role of the Mass Loss

Observational evidence for the mass loss from T Tauri stars identified with young contracting stars has been obtained by Kuhi [595], see also [297]. There are

Table 8.4 Characteristics of stars at the time when T_c is maximum (two lines first) or upon reaching the main sequence (last two lines), $\beta - \alpha$ is defined in (8.6), $\beta_m = P_m/(P + P_m)$, P and P_m are the matter and magnetic pressure, respectively

$\frac{M}{M_\odot}$	t, yr	$\frac{E_M}{E_{grav}}$	$(\beta_m)_c$	$\lg T_{ef}$	$\lg \frac{L}{L_\odot}$	$\lg \frac{R}{R_\odot}$	$\lg T_c$	$\lg \rho_c$	$(\beta - \alpha)_c$	$\lg \frac{L_{grav}}{L}$
0.11	2.9(8)	0.28	0.22	3.41	−3.00	−0.80	6.454	2.52	4.2	0.96
0.12	3.8(8)	0.27	0.20	3.42	−3.01	−0.82	6.520	2.60	4.2	0.85
0.12	7.6(9)	0.27	0.20	3.30	−3.72	−0.94	6.457	2.94	8.43	0.01
0.13	2.9(9)	0.25	0.19	3.40	−3.20	−0.88	6.575	2.81	5.13	0.01

observational data (see, for example, [251]) providing evidence for the matter outflow from some young stars to have the form of bipolar flows (see reviews in [366]). This may be due to the presence of protoplanetary disks [686, 972].

An empirical inclusion of mass loss in evolutionary calculations of stars contracting to the main sequence has been made in [367]. The mass flux has been specified in the form

$$\frac{dM}{dt} = -\frac{\alpha R^3}{M}. \tag{8.9}$$

We measure the stellar mass M and radius R in solar units, time t in years, α in $M_\odot$/yr. For the solar wind $\alpha = 3 \times 10^{-14}$ $M_\odot$/yr. For T Tauri stars the mass flux may be greater by several orders of magnitude. The evolutionary tracks of stars with initial masses of 2.93 and 2.31 $M_\odot$, various α, and with chemical composition $x_H = 0.739$, $x_{He} = 0.24$, $x_Z = 0.021$ are shown in Fig. 8.3, from [367]. Contrary to [485], where $l = \rho/2|\nabla\rho|$, the mean free path of the convective element in the mixing length theory is twice the pressure scale height: $l = 2P/|\nabla P|$. Deuterium burning is also examined, with initial concentration of deuterium taken to be equal to the earth concentration: $x_{2D}/x_H = 1.4 \times 10^{-4}$ [575]. As shown in [367], the lines of equal age (see Fig. 7.6) in the HR diagram are not very sensitive to the mass loss rate determined by α.

8.2 Evolution of Rapidly Rotating Stars on Gravitational Contraction Stages

The rotation velocities of T Tauri stars are difficult to determine by reason of enhanced broadening of emission lines. An estimate of rotation velocity for such stars has been made from narrow absorption lines [468] and interpreting observations of the FeI fluorescence line with $\lambda\lambda$ 4063, 4132, [1039]. This estimate turned out to be $\langle v \sin i \rangle = 20 - 65$ km s^{-1}.

The polytropic equation of state $P = K\rho^\gamma$ with $\gamma = 4/3$ for stars with mass 3–12 $M_\odot$ in [216] and $\gamma = 5/3$ for $M \leq 1$ $M_\odot$ in [712] has been used in theoretical studies of the evolution of rapidly rotating stars at the stage of gravitational contraction. A fixed distribution of angular momentum has been studied in [216],
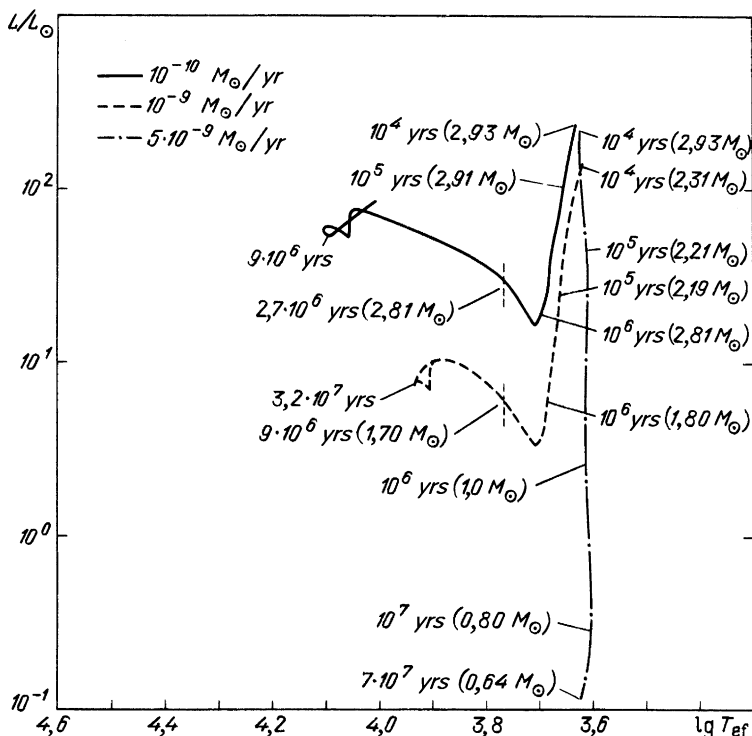
Fig. 8.3 Evolutionary track in the HR diagram for contracting stars with mass loss including the deuterium burning. The initial masses are 2.93 $M_\odot$ and 2.31 $M_\odot$. The *dashed vertical line* indicates the point where the star stops having outer convection zone and continues to evolve with a constant mass. The masses and ages of the models indicated by pointer are also given in the figure. The pointers on the left of the figure (without mass indication) mark the zero-age main sequence

while in [712] the rotation has been taken to be solid-body and critical[1] throughout the evolution. In this section we follow [167, 168], where an exact equation of state for normal chemical composition is used with a full description of ionization states and radiation pressure (see Sect. 1.1, Vol. 1). A distribution of the effective temperature over the stellar surface is obtained by fitting a thin radiative envelope to the convective core on the poles and at the equator separately. Evolutionary stages of fully convective stars are considered, with entropy and angular velocity being constant over the star. The total angular momentum is taken to be constant during the evolution. A constant entropy under conditions of well-developed convection is obvious, because convection in deep stellar layers is carrying heat very effectively.

---

[1] For a critically rotating star, the centrifugal force at the equator counterbalances the surface gravity.

Thus, a very small excess of the temperature gradient over the isentropic state is enough to carry almost all heat flux over the star (see Sect. 3.1, Vol. 1). The constancy of the angular velocity remains to be proved.

8.2.1 On the Distribution of Angular Velocity of Rotation

During evolution, a star undergoes contraction, expansion and mixing due to the meridional circulation and convection. In the presence of differential rotation a turbulent instability may develop. All these phenomena result in a redistribution of angular momentum in the star. The viscosity due to microscopic phenomena tends to equalize the angular velocity, but its magnitude is usually small.

For the case of axial symmetry, the equation in spherical coordinates $(r, 0, \varphi)$ describing changes in rotation velocity v_ϕ in the presence of isotropic viscosity have the form [591]

$$
\frac{\partial v_\phi}{\partial t} + v_r \frac{\partial v_\phi}{\partial r} + \frac{v_\theta}{r} \frac{\partial v_\phi}{\partial \theta} + \frac{v_\phi(v_r + \cot \theta \, v_\theta)}{r}
$$

$$
= \frac{\eta}{\rho} \left[\frac{1}{r^2} \frac{\partial}{\partial r} \left(r^2 \frac{\partial v_\phi}{\partial r} \right) + \frac{1}{r^2 \sin \theta} \frac{\partial}{\partial \theta} \left(\sin \theta \frac{\partial v_\phi}{\partial \theta} \right) - \frac{v_\phi}{r^2 \sin^2 \theta} \right]
$$

$$
+ \frac{1}{\rho} \left[\frac{\partial \eta}{r} \left(\frac{\partial v_\phi}{\partial r} - \frac{v_\phi}{r} \right) + \frac{\partial \eta}{r \partial \theta} \left(\frac{1}{r} \frac{\partial v_\phi}{\partial \theta} - \frac{v_\phi \cot \theta}{r} \right) \right]. \tag{8.10}
$$

Here, $\eta(\rho, \text{T})$ is the viscosity coefficient. For convenience, we shall write hereinafter (8.10) in terms of specific angular momentum j and angular velocity Ω,

$$
j = r v_\phi \sin \theta, \ \Omega = \frac{v_\phi}{r \sin \theta}. \tag{8.11}
$$

Using (8.11), we rewrite (8.10) as

$$
\frac{\partial j}{\partial t} + v_r \frac{\partial j}{\partial r} + \frac{v_\theta}{r} \frac{\partial j}{\partial \theta} = \frac{\sin \theta}{\rho r^2} \frac{\partial}{\partial r} \left(r^4 \eta \sin \theta \frac{\partial \Omega}{\partial r} \right)
$$

$$
+ \frac{1}{\rho \sin \theta} \frac{\partial}{\partial \theta} \left(\sin^3 \theta \, \eta \frac{\partial \Omega}{\partial \theta} \right). \tag{8.12}
$$

The viscosity of matter is usually negligible, and at $\eta = 0$ the angular momentum conservation follows from (8.12) for all fluid rings.

The physical picture is much more complicated in the convectively unstable region. The laminar convection in a rotating fluid has been examined both theoretically and experimentally in many papers (see [429, 1035]). Various forms of angular velocity distribution may correspond to the steady state in which a convectively unstable rotating medium tends to settle down. As can be seen from (8.12), the condition $j = $ const. reduces the left side to zero, while $\Omega = $ const. does the

same for the right side. These conditions cannot be simultaneous at υ_r, $\upsilon_\theta \neq 0$ so that the steady rotation law is intermediate between the conditions $j = $ const. and $\Omega = $ const. The greater the viscosity coefficient, the more solid-body the rotation. The dimensionless parameter characterizing the rotation law,

$$\alpha = \eta/\rho r \upsilon_r \tag{8.13}$$

is the inverse Reynolds number corresponding to the circular velocity $(v_r, \ v_\theta)$. The Reynolds number

$$Re = \frac{vL_d}{v} = \frac{\rho v L_d}{\eta} \tag{8.14}$$

is a dimensionless parameter, determining the character of the hydrodynamic motion, which usually becomes turbulent at large Re (see [591], and Sect. 3.1.3, Vol. 1); η and v are coefficients of the dynamic and the kinematic viscosity, respectively, related by $\eta = \rho v$. L_d is the characteristic scale of the flow. For a steady state, we have $\Omega = $ const. at $\alpha \gg 1$, and we obtain $j = $ const. at $\alpha \ll 1$. According to the numerical calculations in [1035], the rotation is almost uniform at $\alpha = 5$, while at $\alpha = 0.04$ the angular momentum per unit mass is constant over almost the total volume, except for a central region, where $r \to 0$, $\alpha \to \infty$ and $\Omega = $ const.

Convection is always turbulent in stars due to a low viscosity and large characteristic scales (see Sect. 3.1.3, Vol. 1). Also, this scale is usually much smaller than the characteristic core size. Application of numerical modeling is almost impossible here because even for the case of a laminar convection, the computations can incorporate only a small number of convective cells. The microscopic viscosity in stars is so small that a state with $j = $ const. is likely to set in over one convective cell. The averaged Ω distribution over the convective core rather than the instantaneous distribution of parameters inside the cell should nevertheless be taken into consideration for a small-scale turbulent convection. The large-scale distribution results from interactions between convective cells which take the form of convective, or turbulent, viscosity.

With the turbulent viscosity coefficient

$$\eta_\mathrm{T} = \rho \upsilon_\mathrm{T} l, \tag{8.15}$$

where υ_T is the mean turbulent velocity, l is the turbulence length scale and α from (8.13) becomes

$$\alpha = \left(\frac{\upsilon_\mathrm{T}}{\upsilon_r}\right)\frac{l}{r}. \tag{8.16}$$

The r/l ratio is nearly equal to the number of convective cells over the length of the convective zone in the star. In the convective core of a star with mass $30M_\odot$ on the main sequence $l/r \approx 0.1$, $\upsilon_\mathrm{T} \approx 2 \times 10^5$ cm s^{-1} [144, 724]. Estimates for the circulation velocity obtained from similarity relations and the theory of solar rotation [335] give $\upsilon_r < 10^3$ cm s^{-1} for a rotation velocity below the rotation limit. Hence, $\alpha \gg 1$, and in calculations $\Omega = $ const. is adopted for the convective core.

Note that the solid-body criterion $\alpha \gg 1$ holds only for $l \ll r$. The notion of turbulent viscosity otherwise has no meaning, and several convective cells arise, all of them having a steady rotation law close to $j = \text{const}$. Nonetheless, just as in a convectively stable zone, a steady state may never be reached here so that evolutionary calculations taking into account the secular change of the angular velocity (see Sect. 6.3.2, Vol. 1) are needed for the determination of the angular velocity distribution at each evolutionary step.

The above considerations hold only under simple assumptions on the axial symmetry, isotropy of turbulent viscosity, absence of magnetic field. All these assumptions may no longer be valid: instabilities break the axial symmetry [334], the presence of a magnetic field gives rise to additional forces acting in the ϕ direction and complicates (8.10) and (8.12). In several convection models an anisotropic viscous-stress tensor arises, differing in principle from a normal viscosity tensor and not becoming zero for the solid-body rotation [564]. All these complicated effects have been studied with the aid of only simplified models [335, 1010]. For $\alpha \gg 1$, the condition $\Omega = \text{const.}$ seems to be the most reasonable in evolutionary calculations.

Observations of the Sun show a slight (15–20%) equatorial acceleration. This property seems to be inherent in all rotating convective regions of stars and planets and arises from interactions of convective vortices with the overall star rotation. The buoyant force of a vortex with angular velocity ω having a positive component in the direction of the overall angular velocity Ω exceeds the same force of a vortex with a negative component. This gives rise to a constant angular momentum flow outward. In a stationary state a differential rotation sets in, when the angular velocity increases outward (along the cylindrical radius) and the angular momentum flux outward is balanced by the flux inward due to the turbulent viscosity effect (see Problem 1). Other types of interaction between convection, rotation and circulation leading to solar equatorial acceleration have been considered in [335, 851, 1011].

8.2.2 Method for Evolutionary Calculations

The star is divided into an isentropic core rotating as a solid body, and a thin envelope consisting of a radiative outermost region and an underlying non-adiabatic convective zone. The equation of state $P(\rho, T)$ and isentropes $T = T_S(\rho)$ have been derived for the composition $x_H = 0.7$, $x_{He} = 0.28$, $x_Z = 0.02$ by use of the approximate formulae for thermodynamic functions from [769]. An error in these formulae approximating the tables [1025] has been corrected according to [1026].

The equations describing the equilibrium of a rigidly rotating ($\Omega = \text{const.}$) self-gravitating stellar core with a barotropic equation of state $P = P(\rho)$ have been solved using a variant of a self-consistent field method, described in [204]. This method is based on an iterative procedure for finding the equilibrium solution by subsequent use of the equilibrium equation in the integral form, and the integral representation of the gravitational potential (see Sect. 6.2.3, Vol. 1). The equation of state is determined by accepting a constant specific entropy S along the core

$P = P_S(\rho)$, and the total angular momentum of the core J was suggested to remain constant during evolution, as well as its mass M. The mass and angular momentum of the envelope had been taken as negligibly small. In order to find the luminosity of the star and its location in the HR diagram, an envelope, taken to the plane approximation with a thickness h well below the radius R, has been fitted to the core. The envelope is taken to be in mechanic and heat equilibrium in the effective gravitational field

$$g_{\text{ef}} = |\nabla(\chi - \phi)|, \quad \text{where} \quad \chi = \int_0^r \Omega^2 r' dr' \qquad (8.17)$$

is the centrifugal potential.

For a rigid rotation we have $\chi = (\Omega^2 r^2/2)$. The envelope is described by equations

$$\frac{dP}{dx} = -\rho g_{\text{ef}}, \quad F = F_{\text{rad}} + F_{\text{conv}}, \quad F_{\text{rad}} = -\frac{4\alpha c T^3}{3\kappa\rho}\frac{dT}{dx}. \qquad (8.18)$$

Here, the convective heat flux is calculated according to the mixing length model (see Sect. 3.1.3, Vol. 1),

$$F_{conv} = c_p\rho\left[-\left(\frac{\partial\rho}{\partial T}\right)_P \frac{g_{ef}}{\rho}\right]^{1/2}\frac{l^2}{4}(\Delta\nabla T)^{3/2}, \qquad (8.19)$$

where the derivative at constant pressure $(\partial\rho/\partial T)_P$ takes account of the variable ionization states. The variable molecular weight $\mu(\rho, T)$ is found from the condition of ionization equilibrium for an ideal non-degenerate gas (8.4) with $r_p = 0$, x is the coordinate in the envelope in the direction of $\nabla(\chi - \phi)$. The calculations for the envelope have been performed with $l = P/|dP/dx| = H_P$. The core model has been constructed for the outer boundary condition $P = \rho = 0$. The resulting error $\sim h/R$ is small for a thin envelope. The opacity κ for (8.18) has been taken from the tables [316], while for $10^{-3} < \tau < 2/3$ the second and third relations in (8.18) have been replaced by the approximate relation from [769], obtained on the basis of a solution of the radiative transfer equation in the Eddington approximation

$$\frac{dT}{dr} = -\frac{3\kappa\rho F}{4acT^3} - \frac{f}{2}T_0 R_0^{1/2} r^{-3/2},$$
$$f = 1 - \frac{3}{2}\tau \quad \text{for} \quad \tau < 2/3 \qquad (8.20)$$
$$= 0 \quad \text{for} \quad \tau \geq 2/3.$$

Here, $T_0^4 = (F/ac)$, and the calculations in [769] have shown that the distribution in a stellar atmosphere depends only weakly on the choice of R_0 and T_0, corresponding to zero optical depth $\tau = 0$ (see also Sect. 2.2.3, Vol. 1). The envelope model is determined uniquely at known T_{ef} and g_{ef}. All envelopes are radiative at $\tau = 2/3$, $T = T_{\text{ef}}$, but soon with increasing τ the radiative gradient begins to

exceed the adiabatic gradient, and convection breaks out. The density is small in the outer layers of the convective envelope so that the heat transfer by convection has a small efficiency, hence, there is a strong non-adiabaticity, and the entropy increases from the surface inwards. On penetrating downwards from the surface, the convective energy transfer grows increasingly effective, and the temperature gradient approaches the adiabatic gradient. The adiabatic regime of the solution is assumed to set in when the condition

$$|\nabla - \gamma_2| \leq 10^{-3}, \quad \nabla = d \ln T / d \ln P \tag{8.21}$$

is satisfied, where

$$
\begin{aligned}
\gamma_2 &= \left(\frac{\partial \ln T}{\partial \ln P} \right)_S \\
&= \left[\left(\frac{\partial \ln P}{\partial \ln T} \right)_\rho - \left(\frac{\partial \ln P}{\partial \ln \rho} \right)_T \left(\frac{\partial S}{\partial \ln T} \right)_\rho \Big/ \left(\frac{\partial S}{\partial \ln \rho} \right)_T \right]^{-1}.
\end{aligned}
\tag{8.22}
$$

The quantity $T_{\mathrm{ef}} = (4 \, F/ac)^{1/4}$ has been selected in such a way as to make the envelope entropy S_0 at the point $\nabla \approx \gamma_2$ equal to the core entropy S. First, the dependence $S_0(g_{\mathrm{ef}}, T_{\mathrm{ef}})$ has been tabulated, then the values of $T_{\mathrm{ef}}(g_{\mathrm{ef}}, S_0)$ have been found by interpolation of these tables. Note that a similar method for fitting envelopes has been applied to constructing models for non-rotating convective low-mass stars [479]. The calculations reveal a weak dependence $T_{\mathrm{ef}}(g_{\mathrm{ef}})$ (Fig. 8.4) and a fair accuracy of the relation $T_{\mathrm{ef}} \sim g_{\mathrm{ef}}^{0.08}$ obtained in [653].

Using the distribution $T_{\mathrm{ef}}(\theta)$ over the stellar surface $R = R(\theta)$ allows as to find the total luminosity
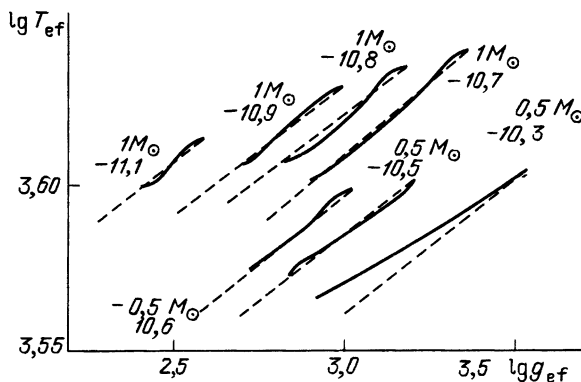
Fig. 8.4 Effective temperature T_{ef} as a function of gravity g_{ef} along stellar surface for models with $0.5 \, M_\odot$, $J = 4 \times 10^{50} \, \mathrm{g \, cm^2 \, s^{-1}}$ and with $1 \, M_\odot$, $J = 14.2 \times 10^{50} \, \mathrm{g \, cm^2 \, s^{-1}}$. *Dashed lines* represent the slope for the dependence obtained in [653]. Each curve is labeled by a number indicating the value of the corresponding parameter $\lg \rho_0$ (see Tables 8.5–8.7)

$$L = \frac{1}{2}\pi\alpha c \int_0^\pi T_{\text{ef}}^4 R \left[R^2 + \left(\frac{dR}{d\theta}\right)^2 \right]^{1/2} \sin\theta \, d\theta. \tag{8.23}$$

With the luminosity and model energy $\mathscr{E}$, we are in a position to determine the age difference between the two convective models

$$\Delta t = 2\frac{|\mathscr{E}_1 - \mathscr{E}_2|}{L_1 + L_2}, \tag{8.24}$$

which may be determined from the mean luminosity between two times "1" and "2". The total energy $\mathscr{E}$ is negative, incorporates thermal, rotational and gravitational energies and has been obtained from the core equilibrium computations (the envelope energy being ignored),

$$\mathscr{E} = -\frac{1}{2}\int \phi \, dm + \frac{1}{2}\Omega^2 \int r^2 \sin^2\theta \, dm + \int E(\rho, S) \, dm$$

$$dm = 2\pi\rho r^2 \sin\theta \, dr d\theta. \tag{8.25}$$

Relations for the specific internal energy $E(\rho, T)$ for the mixture of an ideal gas with radiation, taking into account incomplete ionization, are given in Sect. 1.1, Vol. 1.
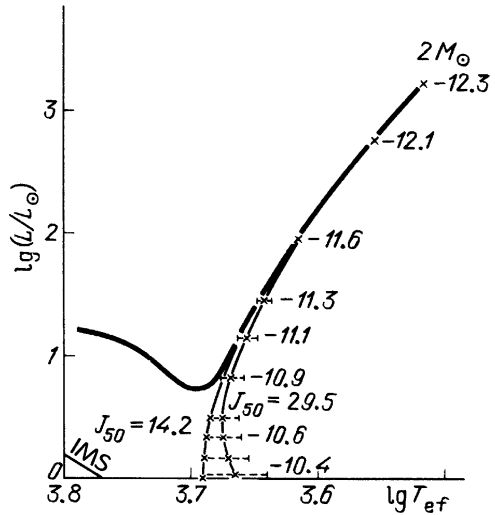
8.2.3 Calculation Results

Calculation of non-rotating star models, comparison with the results [367, 462, 485] together with a test by the Henyey method under the same physical assumptions, reveals that the accuracy of the above method is within 5%, providing the envelope thickness does not exceed $0.3R$, and the radiative core mass is not above 25% of the stellar mass. For stars with masses of 10, 2, 1, $0.5M_\odot$, the envelopes are thin if $L < 4 \times 10^4$, 2000, 100, $50L_\odot$, respectively. The main calculational results are shown in Figs. 8.5 and 8.6, and Tables 8.5–8.7 taken from [167]. For comparison, note that the angular momentum of the Sun in solid-body rotation is 1.6×10^{48} g cm^2 s^{-1} [15]. The entropy has been characterized by the matter density $\rho_0 (\lg \rho_0)$ at $T = T_0$, $\lg T_0 = 3.3$.

The results of evolutionary calculations for stars with $M = 0.5, 1, 2M_\odot$ are given in Tables 8.5–8.7, respectively. Tabulated are time dependences of the polar R_p and equatorial R_e radii, central temperature T_c and central density ρ_c, luminosity L, effective temperature at the pole T_p and at the equator T_e. Given also are equatorial rotation velocities v_{eq} and relative envelope thicknesses h/R_e. A rotating star turns out to have a lower temperature and a higher luminosity than a non-rotating star with the same entropy. For the last model in Table 8.5 with $M = 0.5M_\odot$ and the maximum oblateness $R_e/R_p = 1.6$ (compare Fig. 8.7 for $1M_\odot$) the increase in luminosity is 25%. The effective acceleration is, for this model, $\sim$24 times lower
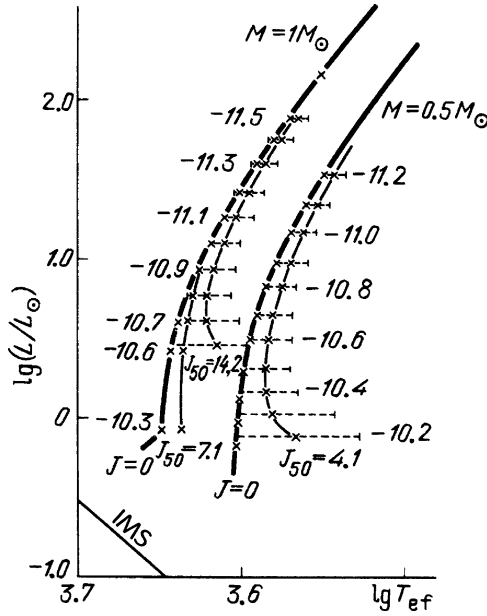
Fig. 8.5 Evolutionary tracks for models of contracting stars with $M = 0.5\,M_\odot$ and $1\,M_\odot$ at diverse values of the angular momentum J_{50} (in $10^{50}\,\mathrm{g\,cm^2\,s^{-1}}$) plotted for mean effective temperatures of stars. *The heavy line* represents the results of the calculations obtained using the Henyey method for non-rotating stars, the crosses correspond to models calculated by the described method. The numbers indicate the values of $\lg \rho_0$ parameterizing the core entropy. *The dashed horizontal lines* mark the effective temperature dispersion over the rotating star surface. *The line labeled* IMS is the initial main sequence for a non-rotating star with $X_H = 0.70$ and $X_Z = 0.02$

Fig. 8.6 Tracks for models with $2\,M_\odot$. The notation is the same as in Fig. 8.5. The radiative core formation causes the star to pass onto the horizontal branch of the track

Table 8.5 Results of evolutionary calculations for a star of 0.5 $M_\odot$

$\lg \rho_0$	$\frac{R_e}{R_\odot}$	$\frac{R_p}{R_\odot}$	T_c, K	ρ_c, g cm^{-3}	$\frac{L}{L_\odot}$	T_e, K	T_p, K	t, yr	v_{eq}, km s^{-1}	$\frac{h}{R_e}$	J g cm^2 s^{-1}
−11.3	20.4		2.47(5)	1.16(−3)	53.8	3475		0	0	0.35	
−11.0	9.03		4.87(5)	8.6(−3)	14.4	3750		8.06(3)	0	0.12	
−10.7	4.44		9.35(5)	5.96(−2)	4.14	3920		6.0(4)	0	0.045	0
−10.4	2.36		1.72(6)	0.36	1.28	4020		3.70(5)	0	0.020	
−10.2	1.62		2.50(6)	1.07	0.609	4020		1.10(6)	0	0.012	
−11.3	21.8	20.3	2.4(5)	1.12(−3)	55.5	3400	3470	0	24.5	0.39	
−11.0	9.86	8.94	4.66(5)	8.05(−3)	14.9	3640	3750	7.50(3)	41.6	0.16	
−10.8	5.09	4.35	8.57(5)	0.0523	4.39	3740	3930	5.48(4)	72.9	0.068	4.10(50)
−10.4	2.97	2.28	1.49(6)	0.292	1.45	3720	4010	3.04(5)	127	0.045	
−10.2	2.47	1.54	2.08(6)	0.832	0.773	3365	4040	8.13(5)	193	0.25^a	

[a]h is large only near equator owing to a decrease in g_{ef}.

at the equator than at the pole. The deviation of the evolutionary tracks to the left (Figs. 8.5 and 8.6, see also Figs. 7.6a, 7.6b and 8.3) arises from the growth of the radiative core and cannot be described by this method. A radiative core treatment should include the non-adiabatically, non-stationary circulation, redistribution of angular momentum and use of the full form of the evolutionary equations, where changes in the distribution of circulation velocities and angular momentum distribution are calculated at each evolutionary step in the same way as changes of the chemical composition (see Sect. 6.3.2, Vol. 1).

The time for a rotating star to contract to the state with a given entropy somewhat decreases because of increasing the luminosity of models with the same S. A rotating star, however, has a lower central temperature and density than a non-rotating star with the same S, so it reaches the main sequence having less entropy and luminosity than the non-rotating star. Approximate calculations of uniformly rotating stars on the main sequence show that the difference in luminosity increases with decreasing mass [370, 794]. If we extrapolate the results [794], we shall have for $M = 0.5 M_\odot$ that a critically rotating star on the main sequence turns out to have a luminosity of 1.6 times lower than the non-rotating star. In addition, a rotating star radiates more heat in its pre-main-sequence phase, so the critical rotation nearly doubles its time of approach to the main sequence.

8.3 Models for the Matter Outflow from Young Stars

The mechanisms of quasistationary matter outflow observed in various stars [289, 595] may be divided into four categories:

(1) Outflow under the effect of the light pressure at small and large optical thicknesses of the outflowing region of the envelope

Table 8.6 Evolution of a star of $1\,M_\odot$

$\lg \rho_0$	$\frac{R_e}{R_\odot}$	$\frac{R_p}{R_\odot}$	T_c, K	ρ_c, g cm^{-3}	$\frac{L}{L_\odot}$	T_e, K	T_p, K	t, yr	v_{eq}, km s^{-1}	$\frac{h}{R_e}$	J g cm^{-2} s^{-1}
−11.5	21.7		4.15(5)	1.34(−3)	83.6	3760		0	0	0.21	
−11.2	10.5		7.88(5)	9.23(−3)	26.2	4040		1.5(4)	0	0.10	0
−10.9	5.23		1.54(6)	0.0669	8.02	4270		1.1(5)	0	0.034	
−10.6	2.73		2.91(6)	0.444	2.52	4420		6.5(5)	0	0.015	
−10.3	1.51		5.24(6)	2.52	0.80	4450		3.6(6)	0		
−11.5	22.0	21.7	4.12(5)	1.33(−3)	84.3	3740	3760	0	15.8		
−11.2	10.75	10.5	7.80(5)	9.03(−3)	26.4	4010	4040	1.5(4)	27.8		
−10.9	5.44	5.20	1.50(6)	0.0642	8.13	4180	4270	1.1(5)	51.3		7.1(50)
−10.6	2.92	2.69	2.76(6)	0.412	2.55	4285	4410	6.4(5)	93.4		
−10.3	1.70	1.48	4.81(6)	2.22	0.83	4260	4440	3.3(6)	162		
−11.5	23.05	21.6	4.03(5)	1.29(−3)	85.7	3680	3760	0	31.7	0.30	
−11.2	11.5	10.4	7.46(5)	8.50(−3)	27.1	3920	4040	1.4(4)	55.1	0.12	
−10.9	6.12	5.12	1.39(6)	0.0575	8.57	4040	4260	9.7(4)	100	0.054	14.2(50)
−10.7	4.25	3.26	2.04(6)	0.192	4.04	3990	4365	3.1(5)	150	0.044	
−10.6	3.66	2.62	2.44(6)	0.341	2.79	3860	4395	5.4(5)	184	0.044	

Table 8.7 Evolution of a star of $1 M_\odot$

$\lg \rho_0$	$\frac{R_c}{R_\odot}$	$\frac{R_p}{R_\odot}$	T_c, K	ρ_c, g cm^{-3}	$\frac{L}{L_\odot}$	T_e, K	T_p, K	t, yr	v_{eq}, km s^{-1}	J g cm^{-2} s^{-1}
−12.3	127		1.79(5)	2.86(−5)	1680	3280	3280	0		
−12.1	61.4		3.09(5)	1.43(−4)	567	3600		5.14(2)		0
−11.6	18.0		9.15(5)	3.62(−3)	85.9	4147		1.26(4)		
−11.3	9.22		1.73(6)	2.43(−2)	29.4	4436		7.28(4)		
−11.0	4.69		3.55(6)	0.175	9.6	4704		4.31(5)		
−10.7	2.43		6.43(6)	1.22	3.05	4903		2.53(6)		
−10.4	1.33		1.18(7)	7.40	0.94	4953		1.40(7)		
−12.3	128	127	1.78(5)	2.86(−5)	1680	3276	3280	0	4.34	
−12.1	61.6	61.4	3.11(5)	1.44(−4)	563	3590	3601	4.70(2)	6.34	
−11.6	18.2	18.0	9.12(5)	3.59(−3)	86.1	4139	4147	1.28(4)	16.0	1.419(51)
−11.3	9.32	9.20	1.72(6)	2.40(−2)	29.5	4422	4436	7.24(4)	29.3	
−11.0	4.78	4.67	3.30(6)	0.171	9.67	4674	4703	4.23(5)	55.3	
−10.7	2.52	2.41	6.25(6)	1.17	3.08	4844	4901	2.45(6)	104	
−10.4	1.41	1.31	1.13(7)	6.86	0.98	4867	4949	1.16(7)	186	
−12.3	129	127	1.78(5)	2.84(−5)	1680	3260	3280	0	9.08	
−12.1	62.3	61.4	3.09(5)	1.43(−4)	566	3577	3600	4.66(2)	13.2	
−11.6	18.5	18.0	8.99(5)	3.52(−3)	86.8	4111	4146	1.22(4)	33.2	2.953(51)
−11.3	9.65	9.14	1.67(6)	2.31(−2)	27.5	4373	4434	7.18(4)	60.2	
−11.0	5.10	4.61	3.15(6)	0.159	9.90	4574	4699	4.09(5)	112	
−10.7	2.84	2.36	5.75(6)	1.03	3.22	4632	4891	2.22(6)	207	
−10.4	1.78	1.27	9.80(6)	5.55	1.06	4345	4932	1.10(7)	371	

Fig. 8.7 The surface shape for a contracting star with $1\,M_\odot$ and $J_{50} = 14.2$ at various times of its evolution. Indicated are $\lg \rho_0$ values (see Table 8.6)
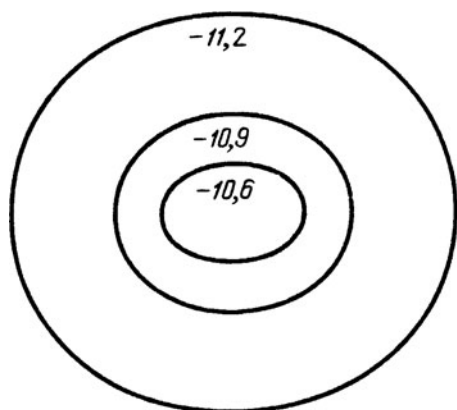
(2) Non-thermal heating and expansion of corona
(3) Rotation mechanism of outflow
(4) Outflow from stellar envelopes owing to the energy release in recombination of atoms and molecules

The role of the rotational mechanism is far from clear because the observable angular velocities are below their critical values. This mechanism seems to be the most important in non-stationary stages of evolution (see Chap. 10). The first of these four mechanisms is due to a large luminosity of the star and is important for very bright blue massive stars and for giants or supergiants at late evolutionary stages (see Chap. 9). Stars of low mass and luminosity, including young contracting stars, have convective envelopes that give rise to non-thermal heating of corona and to its solar wind-like outflow. Recombination effects reduce the adiabatic index down to low values $\gamma_1 < 4/3$ because of transformations between the kinetic energy of particles, and an energy of recombination and ionization, and may thus become important for the mass loss during the earliest stages of star formation. The adiabatic index γ_1 is defined as follows

$$\gamma_1 = \left(\frac{\partial \ln P}{\partial \ln \rho} \right)_S$$

$$= \left(\frac{\partial \ln P}{\partial \ln \rho} \right)_T - \left(\frac{\partial \ln P}{\partial \ln T} \right)_\rho \left(\frac{\partial S}{\partial \ln \rho} \right)_T \bigg/ \left(\frac{\partial S}{\partial \ln T} \right)_\rho, \qquad (8.26)$$

see Sect. 1.1, Vol. 1. It should be noted that the mechanism of mass loss under the effect the of the light pressure is very important for forming massive stars with $M > 9\,M_\odot$ and leads to the dependence (7.30). Consider models of outflowing stars losing mass via the second and fourth of the four mentioned mechanisms.

8.3.1 Outflowing Bipolytropic Models [170]

Consider a star characterized by an equation of state of the form

$$P = K_2\rho^{1+1/n_2} \text{ for } \rho < \rho_a, n_2 \gg 1; \tag{8.27}$$

$$P = K_1\rho^{1+1/n_1} \text{ for } \rho > \rho_a, \tag{8.28}$$

where

$$K_1\rho_a^{1/n_1} = K_2\rho_a^{1/n_2}.$$

A similar equation of state is determined by the gas properties including recombination. The specific thermal energy of this gas is

$$E = K_2 n_2 \rho^{1/n_2} \text{ for } \rho < \rho_a, \tag{8.29}$$

$$E = K_1(n_2 - n_1)\rho_a^{1/n_1} + K_1 n_1 \rho^{1/n_1} \text{ for } \rho > \rho_a. \tag{8.30}$$

Consider a star with mean density $\overline{\rho}$ such that $\rho_a \ll \overline{\rho}$. For a purely polytropic star of mass M and radius R, characterized by the equation of state (8.28) for all densities, the total energy ϵ is determined by [617] (see Sect. 10.1)

$$\epsilon = -\frac{3 - n_1}{5 - n_1} \frac{GM^2}{R}. \tag{8.31}$$

Here, the zero energy corresponds to the stellar matter energy at zero density with no gravitational interaction. If the mass of the envelope with $\rho < \rho_a$ is negligible, then the total energy of the star characterized by the bipolytropic equation of the state (8.27) and (8.28) will be written as

$$\epsilon = (n_2 - n_1)K_1\rho_a^{1/n_1} M - \frac{3 - n_1}{5 - n_1} \frac{GM^2}{R}. \tag{8.32}$$

It can be seen from (8.32) that at a sufficiently high n_2 the total energy becomes positive, and a run-away to infinity becomes energetically allowable. If $n_1 < 3$, then most of the mass will be in stable equilibrium even at a positive total energy (see Chap. 12), while for the matter at $\rho < \rho_a$ the outflow is still possible. When the ratio $\rho_a/\overline{\rho}$ is sufficiently small, the mass loss rate $\dot{M}$ is so low that the major part of the stellar mass is in static equilibrium, and the outflow proceeds in a quasistationary regime with velocity distribution

$$u = -\frac{\dot{M}}{4\pi\rho r^2}. \tag{8.33}$$

In a stellar envelope at $\rho < \rho_a$ with a stationary radial outflow the Bernoulli integral holds [591]

$$H = \frac{u^2}{2} + E + \frac{P}{\rho} - \frac{GM}{r} = \frac{u^2}{2} + (n_2 + 1)K_2\rho^{1/n_2} - \frac{GM}{r}. \qquad (8.34)$$

In order for the condition $\rho \to 0$ as $r \to \infty$ to be satisfied, the solution (8.33), (8.34) has to go through a critical sonic point where the relations

$$u_{cr}^2 = u_{s, cr}^2 = \frac{n_2 + 1}{n_2}K_2\rho_{cr}^{1/n_2},$$

$$u_{cr}^2 = \frac{GM}{2r_{cr}}, \qquad (8.35)$$

are valid. Here, the sound velocity $u_s = (\partial P/\partial \rho)_{K_2}^{1/2}$. To construct a model of a static star with envelope outflow, the solution for the core should be fitted to the solution (8.33) and (8.34) for the envelope in such a way that the density ρ and pressure P are continuous, and the velocity u is very low.

For the case of a barotropic equation of state $P(\rho)$, the equilibrium equation for a static core has an integral yielded by the Bernoulli integral (8.34) with $u \to 0$. The integral H is to be evaluated on the boundary of the static core $r = R$, where we set approximately $\rho = \rho_a, u \ll u_s$, and

$$H = (n_2 + 1)K_2\rho_a^{1/n_2} - \frac{GM}{R}. \qquad (8.36)$$

Inserting (8.35) into (8.34), we express H in terms of the critical point radius r_{cr}:

$$H = \frac{2n_2 - 3}{4}\frac{GM}{r_{cr}}. \qquad (8.37)$$

Combining (8.36) and (8.37) gives the radius $r_{cr}(M, R)$ which, in turn, allows as to find, using (8.35) and (8.33), the mass flux

$$\dot{M} = -4\pi\rho_{cr}r_{cr}^2 u_{cr} = -4\pi r_{cr}^{1.5-n_2}\left[\frac{n_2}{2(1 + n_2)}\right]^{n_2}\frac{(GM)^{n_2+0.5}}{\sqrt{2}K_2^{n_2}}$$

$$\approx -\frac{4\pi}{e}r_{cr}^{1.5-n_2}\left(\frac{GM}{2K_2}\right)^{n_2+0.5}\sqrt{K_2}, \; n_2 \gg 1, \qquad (8.38)$$

$$r_{cr} = \frac{2n_2 - 3}{4}GM\left[(n_2 + 1)K_2\rho_a^{1/n_2} - \frac{GM}{R}\right]^{-1}. \qquad (8.39)$$

From the theory of polytropic stars we have [269] (see Sect. 10.1)

$$R = \left[\frac{(n_1 + 1)K_1}{4\pi G}\right]^{(n_1/(3-n_1))}\left(\frac{M}{4\pi M_{n_1}}\right)^{(1-n_1)/(3-n_1)}\xi_{n_1}, \qquad (8.40)$$

where ξ_n, M_n are dimensionless quantities depending only on n. With (8.39) and (8.40), the function $\dot{M}(M, R)$ becomes

$$\dot{M} = -\pi \left(\frac{e}{K_2 \rho_a^{1/n_2}} \right)^{3/2}$$

$$\times (GM)^2 \rho_a \left\{ 1 - \frac{G(4\pi M_{n_1})^{(1-n_1)/(3-n_1)}}{n_2 K_1 \rho_a^{1/n_1} \xi_{n_1}} \right.$$

$$\times \left. \left[\frac{4\pi G}{(n_1 + 1)K_1} \right]^{n_1/(3-n_1)} M^{2/(3-n_1)} \right\}^{n_2 - 1.5}. \qquad (8.41)$$

The outflow from the stellar envelope requires that the condition $H > 0$ must be satisfied, which is equivalent to the condition $(\partial\epsilon/\partial M)_K \geq 0$ at $n_2 \gg 1$, if (8.40) and (8.42) are taken into account. At $H = 0$ the energy ϵ is positive and $\partial\epsilon/\partial M = 0$:

$$\epsilon = \epsilon_0 = \frac{2GM^2}{(5 - n_1)R} \quad \text{at } H = 0; \ M = M_2. \qquad (8.42)$$

At fixed $n_1 < 3$ and $n_2 \gg 1$ bipolytropic models fall into three types depending on the stellar mass M

$$(1) \ M > M_1, \ \epsilon < 0, \ \partial\epsilon/\partial M < 0, \ H < 0 \qquad (8.43)$$

are stable static models with negative total energy;

$$(2) \ M_2 < M < M_1, \ 0 < \epsilon < \epsilon_0, \ \frac{\partial\epsilon}{\partial M} < 0, \ H < 0 \qquad (8.44)$$

are static models with positive total energy. The run-away to infinity is energetically allowable for the matter, but models are stable against small perturbations (metastable as a whole), and the run-away implies penetrating through a potential barrier;

$$(3) \ M < M_2, \ 0 < \epsilon_0 < \epsilon, \ \frac{\partial\epsilon}{\partial M} > 0, \ H > 0 \qquad (8.45)$$

are quasisteadily outflowing models (there are no strictly static models here, but most of the mass is in almost static equilibrium since $\dot{M}$ is low at low ρ_a).

The value of M_1 may be found from (8.32) with $\epsilon = 0$, and M_2 from (8.36) with $H = 0$, using (8.40). The condition that the critical radius r_{cr} be outside the star

$$r_{cr}/R > 1 \qquad (8.46)$$

is necessary for applying the approximate evaluation of $\dot{M}$ in (8.41). It follows from (8.39) and (8.40) that (8.46) is valid at

$$y = \left(\frac{M}{M_2} \right)^\kappa = \frac{GM/R}{(n_2 + 1)K_2 \rho_a^{1/n_2}} > \frac{2}{n_2 + 0.5}, \quad \kappa = \frac{2}{3 - n_1}. \qquad (8.47)$$

With y from (8.47) and (8.36), we may rewrite (8.41) in the form

$$\dot{M} = -aM^2(1-y)^{n_2-1.5} = -aM_2^2 y^{2/\kappa}(1-y)^{n_2-1.5},$$

$$a = \pi\left(\frac{e}{K_2\rho_a^{1/n_2}}\right)^{3/2} G^2\rho_a,$$

$$aM_2^2 = \pi e^{3/2}(n_2+1)^{3/2}\rho_a R_2^2 \sqrt{\frac{GM_2}{R_2}}. \tag{8.48}$$

Obviously, the maximum in $\dot{M}$ from (8.48) occurs at

$$y = \frac{2/\kappa}{n_2 - 1.5 + 2/\kappa}, \qquad \left(\text{with} \quad \frac{dy}{dM} = \kappa\frac{y}{M}\right). \tag{8.49}$$

At $\kappa > 1$ ($n_1 > 1$) the condition (8.47) stops being valid before $\dot{M}$ reaches a maximum. On the boundary of the validity condition (8.47) the mean stellar density is of order ρ_a and so, as the adiabatic index γ_1 from (8.27) and (8.26), ($\gamma_1 = 1 + (1/n_1)$) is close to unity, the star turns out to be unstable and runs away on the dynamical time scale. This run-away takes place somewhat earlier than the equality in the condition (8.47) is reached. For outflowing stars, just near the boundary $\partial\epsilon/\partial M = 0$, $y = 1$, the value of $\dot{M}$ is small but increasing as the outflow proceeds and M decreases. As the stellar mass reduces by a factor of $(n_2/2)^{1/\kappa}$, the outflow turns into run-away of the whole star. Note that during the mass loss the outflow and run-away velocities remain always of the order of the sound velocity u_s from (8.35) corresponding to the density ρ_a, with the exception of stars with masses $M \approx M_2$, for which outflowing velocities are small due to a large critical radius in (8.39).

For a star with mass $M < M_2$ the dissipation time is, according to (8.48),

$$\tau \approx \frac{M}{\dot{M}} \approx \tau_{h2}\frac{\bar{\rho}_2}{\rho_a}\left(\frac{4}{3e^{3/2}n_2^{3/2}y^{1/\kappa}(1-y)^{n_2-1.5}}\right) =$$

$$= \tau_h\frac{\bar{\rho}}{\rho_a}\left(\frac{4}{3e^{3/2}n_2^{3/2}y^{3/2}(1-y)^{n_2-1.5}}\right), \tag{8.50}$$

where $\tau_{h2} = R_2/\sqrt{GM_2/R_2}$ is the time of hydrodynamical run-away of the core, $\bar{\rho}_2 = 3M_2/4\pi R_2^3$ is the mean density of a core with mass M_2 and radius R_2; τ_h and $\bar{\rho}$ are the same for $M < M_2$. The minimum in the dimensionless quantity in the latter parentheses (8.50) occurs at $y = 3/2n_2$ and equals $8/9\sqrt{2/3} \approx 0.73$ for $n_2 \gg 1$. The dissipation time of a bipolytopic star with $n_2 \gg 1$ and $\rho_a \ll \bar{\rho}$ is thus always well above the hydrodynamical time of the core, and the applied approximation is therefore correct.

A more complicated 3-polytropic model was used in [303] to mimic the disruption of the neutron star with mass slightly less than the minimal one (see Fig. 11.1).

Note that the behaviour of a 3-polytropic star during this disruption, as well as of the one with a more realistic equation of state, calculated in [303], is well reproduced by the picture of disruption of bi-polytropic stars, described above [170].

8.3.2 Outflowing Models for Isentropic Hydrogen Stars [179]

In the ionization and dissociation region the equation of state $P(\rho)$ has $\gamma_1 < 4/3$ at a constant entropy and even $\gamma_1 < 1$ if the radiation is taken into account. This makes possible the existence of steadily outflowing stable configurations similar to the bipolytropic models (8.45) described above. Fully convective contracting stars in the Hayashi stage are characterized by a constant entropy (Sect. 8.1).

Thermodynamic functions for hydrogen along isentropes are shown in Figs. 8.8–8.11 according to calculations [179]. The entropy values are taken to be $S = 20, 24, 30, 36$ in units

$$\mathcal{R} = k/m_p = 8.317 \times 10^7 \text{ erg g}^{-1} \text{ K}^{-1}. \tag{8.51}$$

A gas has been considered in thermodynamic equilibrium with radiation (see Sect. 1.1, Vol. 1), with ionized, atomic, molecular hydrogen in the ground state taken into account, together with rotational and vibrational excitations of the molecular fundamental term. According to the methods described in [426, 617], a correction is
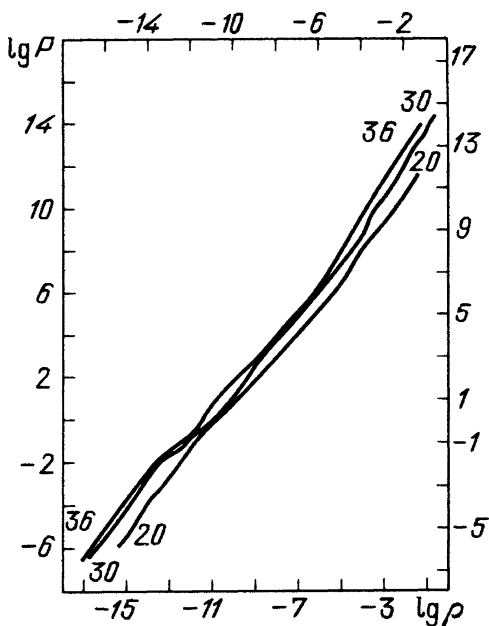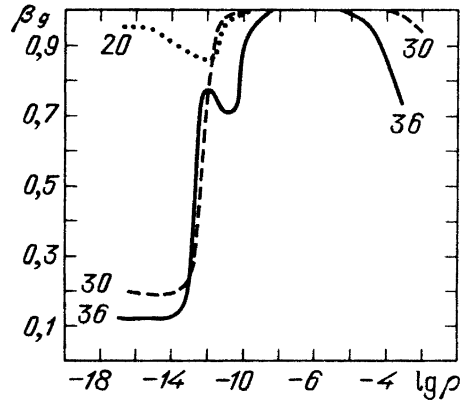

Fig. 8.8 P as a function of ρ along the isentropes $S = 20, 30, 36$
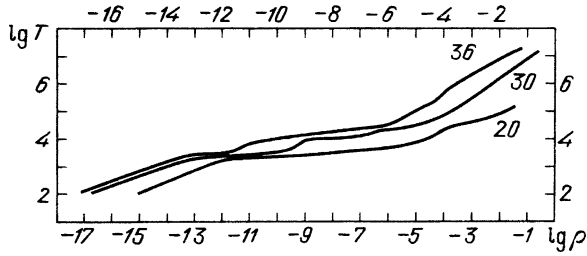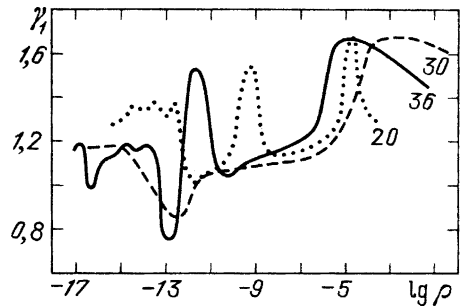
Fig. 8.9 T as a function of ρ along the isentropes $S = 20, 30, 36$

Fig. 8.10 β_g as a function of ρ along the isentropes $S = 20, 30, 36$


Fig. 8.11 γ_1 as a function of ρ along the isentropes $S = 20, 30, 36$

introduced for anharmonicity and interactions between rotational and vibrational degrees of freedom. The ortho- and parahydrogen contents are assumed to be equilibrium.[2] The results of the equation of state calculations [179] are in good numerical agreement with the results in [995, 1025, 1026].

---

[2] In orthohydrogen, nuclear and electron spins are parallel, while in parahydrogen they are antiparallel. The orthohydrogen energetic state is slightly higher than the parahydrogen state; transitions between these states give rise to an emission line of 21 cm in the radio range.

Fig. 8.12 M as a function of ρ_{c0} for static models with $S = 20, 30, 36$. 1, stable branches; 2, intervals with one unstable mode; 3, two; 4, three unstable modes
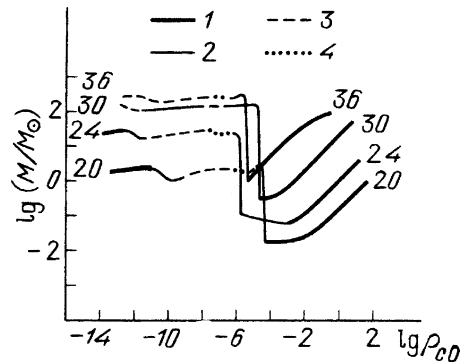
Taking the equilibrium radiation into account, we obtain $\gamma_1 < 1$ for the dissociation region (Fig. 8.11). For a perfect gas with no radiation always $\gamma_1 > 1$ since the temperature increases along isentropes with increasing density.

Static models for hydrogen stars at $S = $ const. and their stability have been examined in [995] with the aid of numerical solution of the equilibrium equations (1a) in Problem 1, Sect. 9.2, and (9.97). Similar calculations have also been made in [179], from where Fig. 8.12 is taken, which represents the mass as a function of central density $M(\rho_{c0})$. In addition to the stability and instability regions obtained in [995], the number of unstable modes is found in [179] by applying the condition of extremal intersection [1075], see also Chap. 12. The function $M(\rho_{c0})$ has a particularity consisting of the presence of a steep fall appearing at $S > 14$ in the region where the major part of the star is in a partial ionization state. No static model has been constructed in [179, 995] for the fall interval. After the fall, the number of unstable modes either decreases by unity, and the model becomes stable (for $S = 20, 30, 36$ in Fig. 8.12), or does not change, and the instability remains (for $S = 24$).

Besides static models, models with stationary outflow analogous to (8.45) have been constructed in [179] to the left of the fall, with a curve $M(\rho_{c0})$ for outflowing models continuously fitted to the static curve $M(\rho_{c0})$ at the low endpoint of the fall (Fig. 8.13). The techniques used for constructing models with outflow are the same as for analogous bipolytropic models and require that the Bernoulli integral H from (8.34) be positive if the zero-point energy is the energy of the molecular hydrogen state. With the known H, writing the relation (8.34) at the critical pont (8.35) where

$$u_{\text{cr}}^2 = (\partial P/\partial \rho)_S = \gamma_{\text{cr}} \frac{P_{\text{cr}}}{\rho_{\text{cr}}} = \frac{GM}{2r_{\text{cr}}}, \qquad (8.52)$$

we can find numerically the critical point parameters and the mass-loss rate $\dot{M}$ from (8.33).

For finding the integral H, the following procedure has been used in [179]. The structure of static cores is calculated for a given entropy by integrating equations of static equilibrium (1a) in Problem 1, Sect. 9.2, and mass conservation (9.97) from

Fig. 8.13 M as a function of ρ_{c0} for outflowing models. The *dashed line* confines the region of stationary outflow, the isentropes $S = 14, 50$ are taken from Fig. 1 in [995]
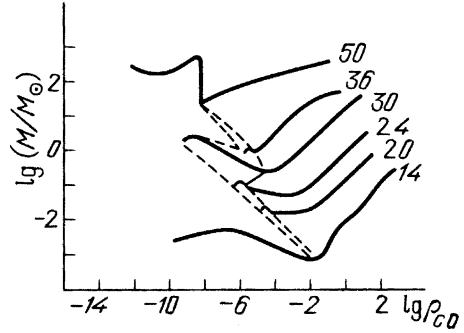
the centre outwards at a given central density ρ_{c0}. The quantity H from (8.34) is evaluated at each step. The possibility to construct a model with static core and stationary envelope outflow analogous to (8.45) requires the following conditions:

1. There must be a shell extended along the radius and having $H \approx \text{const.} > 0$ and a mass much lower relative to the static core mass. The reason is that in a model with outflow there is an intermediate region with $u \ll u_s$ where hydrostatic equations are valid with fair accuracy. The structure of the outflowing star must not depend on the fitting point of two solutions. The constancy of H and a low value of the shell mass will determine the outflowing model unambiguously at given S and ρ_{c0}.
2. The critical radius r_{cr} from (8.52) must exceed the fitting point radius r_b (see (8.46)).
3. The mass m_l of the layer $r_b < r < r_{\text{cr}}$ must be much smaller than the core mass M. This allows use of the Bernoulli integral (8.34) without self-gravitation. The same condition determines a quasistationary character of outflow with the dissipation time of the star $\tau \gg \tau_h$ (see (8.50)).
4. The velocity at the fitting point must be low, $u_b^2/H \ll 1$, which is analogous to the condition 1.
5. Besides condition 3, neglecting the self-gravitation of matter in the flow requires that the inequality

$$\Delta H = G \int_{r_b}^{r_{\text{cr}}} \frac{dm}{r} \ll H \tag{8.53}$$

be satisfied. The outflowing models presented in Fig. 8.13 satisfy all the above conditions. The dependence $H(r)$ for static models with various central densities r_{c0} at $S = 30$ shown in Fig. 8.14 illustrates the outflowing model appearance. The curve $H(r)$ has a plateau for models with

$$\rho_{c,\text{min}} = 8.0 \times 10^{-10} < \rho_{c0} < 3.4 \times 10^{-5} \text{ g cm}^{-3} = \rho_{c,\text{max}} \tag{8.54}$$

and the value $\rho_{c0} = \rho_{c,\text{max}}$ corresponds to the fall of the static curve $M(\rho_{c0})$. Outflowing models do not exist to the right of this fall, while to the left an outflowing solution exists together with much more massive static unstable solutions.
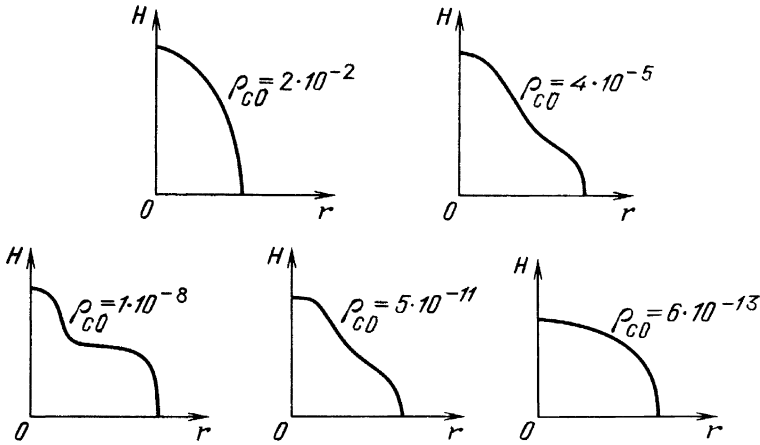
Fig. 8.14 Successive shapes of the dependence of $H = E + P/\rho - Gm/r$ on the current radius of static model along the isentrope $S = 30$ for various ρ_{c0} (qualitative picture). Shown are only portions of $H(r)$ for which $H > 0$

Table 8.8 Models of stationary outflowing isentropic stars

$\frac{S}{\Re}$	ρ_{c0}, g cm^{-3}	$\frac{M}{M_\odot}$	$\frac{r_b}{r_\odot}$	$\frac{H_b}{\Re}$		ρ_b, g cm^{-3}	T_b, K	μ_b
30	8.7(−6)	0.358	629		1.2(4)	7.8(−12)	2100	1.13
30	2.7(−9)	1.594	3178	9300		7.2(−13)	1820	1.27
30	8.05(−10)	1.460	4227		1.3(4)	1.0(−12)	1840	1.74
24	1.8(−6)	0.103	218	2503		9.5(−12)	1897	1.47
24	1.0(−6)	0.107	274	4000		6.6(−11)	1860	1.49
24	5.1(−7)	0.094	365	8800		2.6(−11)	1990	1.42

The subscript "b" denotes quantities at the fitting-point, μ is the molecular weight, $\beta_g = P_g/P$ (see (Sect. 1.1, Vol. 1)), ϵ/M is the specific total energy with respect to molecular hydrogen.

Table 8.8

β_{gb}	$\frac{r_{cr}}{R_\odot}$	$\frac{M}{M_\odot/yr}$	$\frac{10^3 m_l}{M}$	$\frac{10^3 \Delta H}{H}$	$\frac{10^3 u_b^2}{H}$	$\frac{E/M}{10^{12} \text{ erg g}^{-1}}$
0.963	1400	4.5(−5)	3	0.8	0.3	4.16
0.759	4720	3.8(−4)	6	1	5	1.50
0.770	6700	1.1(−3)	30	4	7	1.61
0.969	420	7.5(−6)	0.4	0.2	0.8	1.50
0.958	571	9.3(−6)	0.8	0.4	1	1.18
0.987	882	2.5(−4)	20	4	8	1.39

Parameters of some outflowing models for which conditions 1–5 hold are given in Table 8.8. Minimizing the quantity

$$\eta = \frac{m_l}{M} + \frac{\Delta H}{H_0} + \frac{u_b^2}{H_b} \qquad (8.55)$$

yields the fitting point for models from Table 8.8 and Fig. 8.13, though the results are not very sensitive to the fitting-point shift along the plateau portion of $H(r)$. The dissociation energy is 2.15×10^{12} erg g^{-1} for hydrogen, the ionization energy is 13×10^{12} erg g^{-1}; all the models except the first in Table 8.8 have a negative energy with respect to atomic hydrogen. Comparison reveals that the outflow region along the ρ_{c0} axis in Fig. 8.13 is proportional to the height of the fall on the curve $M(\rho_{c0})$ along the M axis (Fig. 8.12). The fall height is maximized at $S = 30$, when the region of outflowing models is maximum. The disappearance of the fall on the curves $M(\rho_{c0})$ from [995] determines the upper and lower boundaries for outflowing models in Fig. 8.13.

The cores of stars with stationary outflow seem to be dynamically stable, though rigorous methods for stability studies are not yet available. An outflowing star may transform into a static one with a lower mass and higher density, contrary to bipolytropic models where, for the case of a star with stationary outflow, ρ always decreases in time ($\overline{\rho} \sim M/R^3 \sim M^{2n_1/(3-n_1)}$, $n_1 < 3$, see (8.40)), and the star eventually dissipates.

The realization of such outflowing models in nature requires that the protostar matter be additionally heated at sufficiently early phases of protostar formation by cosmic rays or radiation emitted by hot stars forming in the neighbourhood.

8.3.3 Models for Outflowing Coronae of Young Stars

The observed shapes of emission lines H and K of ionized calcium and Balmer lines of hydrogen from T Tauri stars correspond to outflow velocities above 100 km s^{-1}. These values exceed by far the thermal velocities at temperatures of possible formation of these lines [594]. To account for this fact, together with other observable properties of young stars, a model of outflowing corona where cold and dense condensations form owing to the thermal instability development has been examined in [181]. After being formed, the condensations undergo a slowdown under the effect of stellar gravity and produce the observed line emission.

It is assumed that the corona formation is due to the conversion into heat of the mechanic energy flow from the convective envelope. The magnetic field plays an important role in this conversion. In analogy with the most simple models for the solar corona [798], we assume the corona of a young star to be isothermal inside and adiabatic outside. The quantity $\int dP/\rho$ in the Bernoulli integral (8.34) has the form [181,617]

$$\int \frac{dP}{\rho} = E + P/\rho - TS \quad \text{at } T = T_0 = \text{const.}$$
$$= E + P/\rho \quad \text{at } S = S_1 = \text{const.} \tag{8.56}$$

Accordingly,

$$H = H_i = (u^2/2) + E + (P/\rho) - T_0 S - (GM/r) \quad \text{at } T = T_0 \qquad (8.57)$$

$$= H_a = (u^2/2) + E + (P/\rho) - (GM/r) \quad \text{at } S = S_1. \qquad (8.58)$$

The continuity condition for u, ρ and T at the point $r = r_1$, where the transition from isothermal flow to an adiabatic one occurs, yields the relation

$$H_a = H_i + T_0 S_1. \qquad (8.59)$$

The critical point is assumed to be located in the isothermal region where, instead of (8.52), we have

$$u_{cr}^2 = \left(\frac{\partial P}{\partial \rho} \right)_T = \frac{GM}{2r_{cr}}. \qquad (8.60)$$

With the temperature of the isothermal corona T_0 and the integral H_i from (8.58), using (8.60), we may find the critical point parameters u_{cr}, ρ_{cr}, r_{cr} and the mass flow $\dot{M}$ from (8.33). In order to determine the matter velocity at infinity, the entropy S_1 should be specified at the fitting point $r = r_1$:

$$u_\infty^2 = 2(H_i + T_0 S_1). \qquad (8.61)$$

The integral H_i is determined by the specified corona luminosity. To calculate the luminosity when H_i is known, we have to specify a mechanism for corona acceleration and find the temperature, density and velocity distribution in it.

The rapid conversion of the mechanical energy flow $Q(\text{erg s}^{-1})$ into heat is assumed to take place at radius r_b nearly equal to the stellar photosphere radius r_{ph}. The plasma parameters are almost discontinuous at this point, and the temperature is assumed to increase from the photosphere value T_{ph} to the corona value T_0. The conservation laws hold at the heat-discontinuity point [151]:

$$\rho_{b-} u_{b-} = \rho_{b+} u_{b+}, \qquad (8.62)$$

$$P_{b-} + \rho_{b-} u_{b-}^2 = P_{b+} + \rho_{b+} u_{b+}^2, \qquad (8.63)$$

$$\frac{u_{b-}^2}{2} + E_{b-} + \frac{P_{b-}}{\rho_{b-}} + \frac{Q}{4\pi r_b^2 \rho_{b-} u_{b-}} = \frac{u_{b+}^2}{2} + E_{b+} + \frac{P_{b+}}{\rho_{b+}}. \qquad (8.64)$$

The quantities to the left of the discontinuity point (closer to the star) are labeled here by the subscript $(b-)$, to the right by $(b+)$. From (8.58) and (8.33) we have two other equations:

$$\rho_{b+} u_{b+} = \frac{\dot{M}(H_i, T_0)}{4\pi r_b^2}, \qquad (8.65)$$

$$\frac{u_{b+}^2}{2} + E_{b+} + \frac{P_{b+}}{\rho_{b+}} = H_i + T_0 S_b + \frac{GM}{r_b}. \qquad (8.66)$$

With the thermodynamic functions $P(\rho, T)$, $E(\rho, T)$, $S(\rho, T)$ for the ideal gas in equilibrium with radiation, taking into account the incomplete ionization states (see Sect. 1.1, Vol. 1) and given values

$$T_{b-} = T_{ph}, \quad T_{b+} = T_0, \quad r_b = r_{ph}, \quad H_i \tag{8.67}$$

the relations (8.62–8.66) represent five equations for five unknowns

$$\rho_{b-}, \ \rho_{b+}, \ u_{b+}, \ u_{b-}, \ Q. \tag{8.68}$$

The solutions to this system for hydrogen plasma transparent for radiation and characterized by the above thermodynamic functions (see [179]) have been obtained in [181, 182] for several sets of the parameters (8.67) and are given in Table 8.9.

A part (a half or less) of the corona X-ray emission L_{cor} strikes the stellar surface and heats it, forming a hot chromosphere layer with $T_{ch} = (5–10) \times 10^4$ K in addition to the "cold" chromosphere layer with $T_{ch0} \approx 10^4$ K owing its origin to heat conducting effects. The hot chromosphere parameters: temperature T_{ch}, density ρ_{ch}, luminosity L_{ch} and thickness h_{ch} are calculated either from the energy balance of a chromosphere layer with uniform density under the assumption of minimum chromosphere density providing the given cooling rate ([162], first two lines in Table 8.9), or from the condition of equilibrium between the chromosphere and corona pressures ([163], the final three lines in Table 8.9).

The hot chromosphere of T Tauri stars examined in [181] has been discovered by ultraviolet observations from the IUE satellite, and its luminosity has been found to be ~$0.3L_\odot$ in the 1,150–3,100 A range [408] for RU Lupi. Chromosphere and corona parameters and the expected X-ray emission of this star have been evaluated in [182] (last three lines in Table 8.9). Observations in the soft X-ray range

Table 8.9 Model parameters of outflowing **T Tauri** stars

$\frac{r_b}{R_\odot}$	T_{ph}, 10^3 K	T_0, 10^6 K	ρ_{b+}, 10^{-13} g cm^{-3}	u_{b+}, km s^{-1}	$\frac{r_{cr}}{R_\odot}$	u_{cr}, km s^{-1}	ρ_{cr}, 10^{-14} g cm^{-3}	$\dot{M}$, 10^{-8} $M_\odot$/yr
3.5	4.9	1.0	7	67	5.7	129	10	6
2.0	4.9	1.6	6	72	3.6	163	8	2
2.4	4.43	2	1					0.9
2.4	4.43	2.4	1.2					2
2.4	4.43	2.4	1.7					3

L_{ph} is the photosphere luminosity, M_{cor} is the corona mass at $r_b < r < r_c$

Table 8.9

$\frac{L_{ph}}{L_\odot}$	$\frac{L_{cor}}{L_\odot}$	$\frac{M_{cor}}{M_\odot}$	T_{ch}, 10^4 K	ρ_{ch}, 10^{-11} g cm^{-3}	$\frac{L_{ch}}{L_\odot}$	h_{ch}, km	t_1, s	t_2, s
6.36	108	3(−11)	8.9	2	54	1.6	41	9(4)
2.06	14.6	5(−12)	4.6	2	7.3	1.85	108	4(4)
2	0.6		6.0	0.33	0.3	10		
2	2		5.8	0.5	0.7	10		
2	4		6.0	0.67	1.0	6		

from the Einstein [381, 407] and ROSAT [739] satellites have revealed a moderate luminosity $L_X \leq 10^{31}$ erg s^{-1} of T Tauri stars which is well below the values of L_{cor} given in Table 8.9 (see reviews [692, 789]). Observations from the Astron satellite provide evidence for a strong RU Lupi variability in the X-ray range of 2–7 KeV [420]. The weak observed values of the X-ray luminosity of young stars might be due to the strong X-ray absorption in the envelope around them, and their real X-ray luminosity L_{cor} might exceed by far the observed values so that $L_{cor} \geq L_{ch}$, in accordance with [182].

The heat discontinuity (8.62–8.64) for models from Table 8.9 occurs at densities well below the photosphere density $\rho_{b-} \ll \rho_{ph}$ and optical thicknesses $\tau = 10^{-2}$–10^{-3} [181]. In the temperature range of $T = (1$–$3) \times 10^6$ K the cooling function $\Lambda(T)$ erg cm^3 s^{-1} for transparent plasma with normal composition decreases with temperature [313], giving rise to instability with respect to the formation of condensations with lower temperature and higher density.[3] The time for a condensation to form is

$$t_1 \approx \frac{E}{n^2 \Lambda(T)}. \tag{8.69}$$

The minimum size of condensation is determined by the heat conductivity and equals

$$l_{min} \approx \frac{1}{n} \sqrt{1.8 \times 10^{-6} T^{7/2} / \Lambda(T)} \approx 4 \times 10^7 \text{ cm}$$

$$\text{for } n = 10^{11} \text{ cm}^{-3}, T = 10^6 \text{ K.} \tag{8.70}$$

Thermal instability in the solar corona does not develop because of a low density and large value of l_{min}. The time of thermal instability development t_1 is given in Table 8.9 along with the time t_2 for outflowing gas to travel through the characteristic size of a corona [181]. The condition $t_2 \gg t_1$ means that the thermal instability has the time to develop, and cold dense condensations emerge.

The existence of dense chromospheres and coronae in T Tauri stars requires a theoretical explanation for formation in stars with large convective envelopes of a powerful mechanical energy flow comparable with photosphere flow. This phenomenon may have an explanation from the thermodynamical standpoint under the assumption of a high temperature T_m in the region where the mechanical energy flow forms. The efficiency of conversion of the heat flow into mechanical energy flow in a star treated as a heat engine [105] does not exceed

$$\eta < \frac{T_m - T_{ph}}{T_m}, \tag{8.71}$$

and at $T_m \gg T_{ph}$ may be close to unity.

---

[3] The quantity $\Lambda(T) n_e (n_e + n_H)$ erg cm^{-3} s^{-1} represents the energy amount emitted by 1 cm^3 of plasma in 1 s; $\Lambda(T)$ is evaluated in [313].

If the coronal emission of T Tauri stars is equal to or greater than the photosphere luminosity, it may resolve, in part, a contradiction appearing in determining the age of young stellar clusters [105, 167]. The age determined from the turning point of massive stars off the main sequence (see Sects. 9.2 and 9.3) turns out to be less than the age determined as the time of contraction of low-mass stars. These ages are $(4–8) \times 10^8$ and 2×10^9 yr for Hyades; 6×10^6 and 2×10^7 yr for NGC 2264, respectively [588]. When the total bolometric luminosity is several times greater than the photospherical one, this must be taken into account in evolutionary calculations, and the second quantity will then decrease in such a way as to weaken or even remove this contradiction.

8.3.4 On the Phenomenon of Fuor

Several stars are known at present which rapidly increase their luminosity by about a factor ~ 100 and keep this high level for many years. FU Ori was the first star of this kind and gave its name to the phenomenon of fuor [23]. The latter may be attributed to the birth of a young star with sufficiently high mass $M > 3M \odot$ which completes the accretion stage, evaporates its dust envelope after hydrogen ignition, and appears immediately near the main sequence ([622, 1063], see Sect. 7.2). This simple explanation encounters difficulties when applying to the fuor of V1057 Cyg where a T Tauri star had been observed before the outburst [469]. The masses of T Tauri stars are well below the estimates of stellar masses for FU Ori and V1075 Cyg [800] after outburst. To avoid these difficulties, one may assume that V1075 Cyg is a binary containing a T Tauri star and a young star with significantly higher mass which produces the phenomenon of fuor [105, 180]. At the stage of dust envelope the massive star was emitting mostly in the infrared range, while in the optical range its emission was weaker than that of the neighbouring T Tauri star. At present the T Tauri star is essentially, by a factor ~ 100, weaker than its companion, but we may still expect its discovery which is facilitated by strong emission lines, ultraviolet excesses and other peculiarities of T Tauri stars [800]. With the aid of speckle-interferometry observations the T Tauri star has been found to be a binary itself, its companion being an infrared star with insufficiently studied properties [337, 455].

Other fuor models are based on phenomena of non-stationary disc accretion, strongly increasing the star luminosity. In this case, we may expect that the star will return in reasonable time to its previous state.

Problem. Find the equatorial acceleration of a convective star due to buoyancy of eddies.

Solution 8.1. [107, 332]. The eddies, whose projection $\omega_\Omega = \omega \sin \theta$ on the direction of angular velocity $\Omega \parallel OZ$ is positive, are under the action of a larger centrifugal force F_{cf} than those with negative projection

$$F_{cf} \approx \frac{(\Omega r + \Omega r_0)^2}{r} \sin \theta, \tag{8.72}$$

where r is a spherical radius, r_0 is the radius of the eddy.

Larger F_{cf} require smaller pressure P inside the eddy as well as density in order to be in equilibrium with the surrounding medium. Smaller density means larger buoyancy force for rising and smaller sinking force for descending convective eddies. All this leads to a net flux of angular momentum in the direction of entropy decrease, i.e., to the surface of a star with a convective envelope. The part of the pressure deficit inside the eddy, linear to ω, is connected with the part of the centrifugal potential $\Delta \phi_{cf} = \Omega \omega r_0^2 \sin^2 \theta$. The density difference in eddies rotating in opposite directions is obtained from the Bernoulli integral taking into account the enthalpy, the gravitational and centrifugal potentials (see Sect. 6.2.3, Vol. 1), and is equal to

$$\frac{\Delta \rho}{\rho} = \frac{2\Delta \phi_{cf}}{v_s^2} = 2 \sin^2 \theta \, \frac{\Omega \omega r_0^2}{v_s^2}. \tag{8.73}$$

The density is smaller for eddies with positive projection of rotational velocity on the direction of stellar rotation velocity Ω, $v_s^2 = 5P/3\rho$ is the sound velocity squared. The difference of convective velocities v, corresponding to the eddies with opposite rotation follows from (8.73), and the relations for a convective velocity, taking into account the buoyancy acceleration (see Sect. 3.1, Vol. 1)

$$\frac{1}{2}\rho v^2 = \frac{1}{2}\Delta \nabla \rho \, dr^2 g + \frac{1}{2}g\Delta \rho dr, \tag{8.74}$$

with $\overline{dr} = l/2$, and is given by

$$2v \, \Delta v = l \frac{Gm}{r^2} \frac{\Omega \omega r_0^2}{v_s^2} \sin^2 \theta. \tag{8.75}$$

The velocity difference (8.75) corresponds to the projection on the equatorial plane of the flux of angular momentum to stellar surface $\dot{J}_{out}$ through the area unit

$$\dot{J}_{out} \approx \Delta v \rho \omega r_0^2 \sin \theta. \tag{8.76}$$

Differential rotation produced by angular momentum flux (8.76) is smoothed by convective viscosity leading to the angular momentum flux $\dot{J}_{in}$ inside

$$\dot{J}_{in} \approx \eta_{conv} r^2 \sin^2 \theta \, |\nabla \Omega|. \tag{8.77}$$

In the stationary state $\dot{J}_{out} = \dot{J}_{in}$. Supposing that the radiative core inside the star (Sun) rotates rigidly with $\Omega = \Omega_0$ and $|\nabla \Omega| \approx \Delta \Omega / h$, where h is the thickness

of the convective zone, we obtain the following estimation for the equatorial acceleration of the star δ

$$\delta = \frac{\Omega_{\text{eq}} - \Omega_{\text{pole}}}{\Omega} \approx \left(\frac{Gm}{rv_s^2}\right)\left(\frac{r_0}{r}\right)^2\frac{h}{r}\left(\frac{\omega r_0}{v}\right)^2. \tag{8.78}$$

This estimation is sensitive to the choice of v_s and gives, for the Sun [107], $\delta = 2\text{--}20\%$ for $v_s^2 = 10^{14}\text{--}10^{13}\,\text{cm}^2/\text{s}^2$.